Chapter 3

The WA93 Experimental Setup

In this chapter an overview of the experimental setup and its arrangement in the SPS heavy-ion beam-line will be given. The layout of the experimental setup is shown in figure 3.1. The 200 A·GeV sulphur beam enters the beam counter (start detectors) from the left. The target foil, either sulphur or gold, was placed at the entrance of the large dipole magnet. The negatively charged particles, from a nuclear reaction, are bent by the dipole magnet into the acceptance of a tracking system consisting of four position sensitive Multi Step Avalanche Chambers. At the entrance of the magnet a Silicon Drift Detector measures the rapidity distribution of traversing charged particles. Further to the right neutral mesons and photons are measured by the Photon Multiplicity Detector (PMD) and the Lead-Glass Spectrometer. Two layers of Streamer-Tube Detectors measure the position of traversing charged particles in front of the Lead-Glass Spectrometer and serve as a charged particle veto for the Lead-Glass Spectrometer. Behind the photon spectrometer two calorimeters are situated. The Mid-rapidity Calorimeter measures the transverse energy from the nuclear reaction whereas the Zero-Degree Calorimeter measures the forward directed energy. These two calorimeters define together with the start detectors the reaction trigger and the centrality of the collision. First of all the Trigger System, section 3.5, defining the centrality of the heavy-ion collision, is discussed. The trigger system consists of the Beam Counter, section 3.2, and calorimeters. The calorimeters measure the energy of particles in the beam, section 3.3, and transverse to the beam direction, section 3.4.

The main interest of the WA93 experiment [5, 56, 57] is the measurement

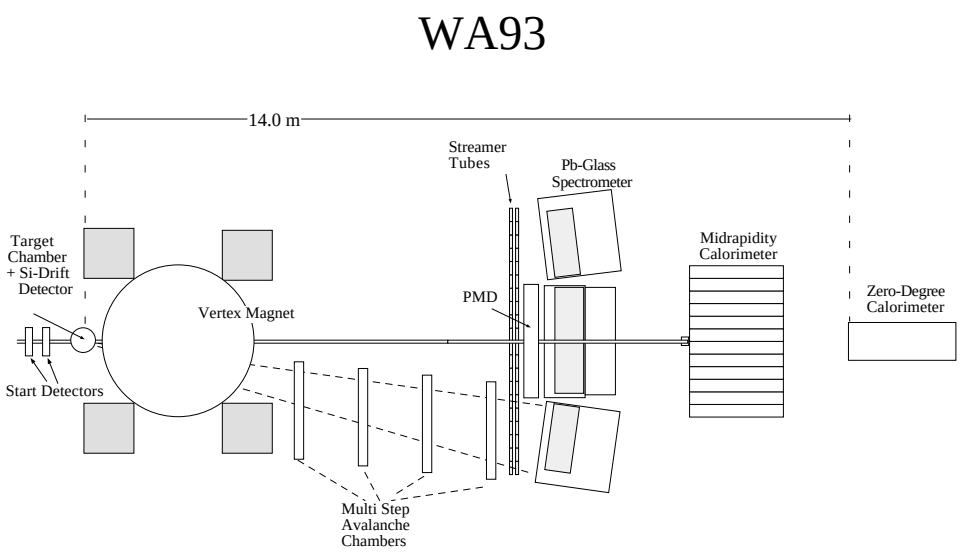

Figure 3.1: *Schematic layout of the WA93 experiment.*

of direct photons. A photon spectrometer consisting of a large array of lead-glass modules, Lead-Glass Spectrometer, section 3.8, and a Photon-Multiplicity Detector, section 3.9, are used to measure the neutral mesons and photons.

Special emphasis will be put on the Charged-Particle Spectrometer; see section 3.10. As has been shown in section 2.4 the measurement of the space-time evolution is a prerequisite for an understanding of the measured direct photon spectra. The charged-particle spectrometer provides the means to do negatively charged-particle intensity interferometry; see section 2.8. It consists of the dipole magnet Goliath and four large-acceptance Multi-Step Avalanche Chambers (MSAC). An extensive description of the design, building, operational requirements, principal of operation, and optical readout of the chambers will be given as the author was actively involved in these subjects.

A new development in which the author took part, enabling direct read-out of the charge at the back of the chamber, is presented in section 3.12. For this purpose a charge-sensitive chip and a fast read-out system, based on Digital Signal Processors, were developed.

The schematic layout of the Data-Acquisition System with special emphasis on the MSAC chambers can be found in section 3.11.

3.1 Production of the CERN Heavy-Ion Beam

To reach the beam energy of 200 A·GeV for sulphur particles and 160 A·GeV for lead particles the atoms are first ionized partially to a high charge state in an ECR-ion source and subsequently linearly accelerated in a 50 MeV LINAC. After the LINAC the ions enter fully ionized the 800 MeV Booster machine, after which they are further accelerated in the 28 GeV Proton Synchrotron (PS) (200 m diameter). Finally the ions enter the Super Proton Synchrotron (SPS) (2.2 km diameter) and get accelerated up to 200 (160) A·GeV, before being extracted into the heavy-ion beam-line leading to the West Area where the WA93 experiment is installed. A complete cycle of accelerating the beam particles and extracting them takes about 19 seconds. During 5 seconds the beam is extracted while for about 2 to 3 seconds during this period a sufficiently constant beam intensity is maintained.

3.2 Beam Counter

The beam counter consists of a halo wall, two quartz-Cherenkov counters and a scintillator paddle. It determines whether a beam particle approaching the target had already undergone interactions upstream producing secondary particles.

The beam from the SPS may have had interactions with rest gas atoms in the vacuum of the beam-line during the transport over a distance of 1 km. The halo wall in this case will mostly register muons. The scintillators in the halo wall are combined in OR-mode $S_{innerhalo}$ and form an inhibit in the off-line analysis package; see section 4.2.

On their way to the target the beam particles pass two quartz-Cherenkov counters viewed by photomultipliers. The presence and charge of the particles can be determined from the energy of the emitted Cherenkov radiation that is proportional to

$$\frac{dE}{dx} = \frac{4 \cdot \pi^2 \cdot Z^2 \cdot e^2}{c^2} \int_{\nu_{min}}^{\nu_{max}} (1 - \frac{1}{\beta^2 \cdot n^2}) \cdot \nu \cdot d\nu \qquad (3.1)$$

where β is the velocity of the particle, n the index of refraction and ν the frequency of the emitted Cherenkov light. The risetime of the photomultiplier signals is fast, in the order of several nano-seconds. The narrow pulse width of the signal allows to count the individual particles in the beam flux of $\sim 10^6 - 10^7$ Hz. Two thresholds are set for the Cherenkov counters. A lower threshold S_{low} is set just above the noise level and an upper threshold

S_{high} is set just above the expected signal in order to prevent pile up arising from several beam particles entering the setup.

In order to check the positioning of the beam, a scintillator paddle of the dimension 64×50 mm^2 and 5 mm thick, with a 3 mm diameter hole, was placed 0.36 m downstream. In case of a signal, $S_{littleveto}$, in the paddle, due to a reaction in the start counters upstream or a bad beam positioning on the target, the beam trigger was inhibited. The validity of a beam particle exactly centered on the target was logically defined as

$$S_{validbeam} = (S^1_{low}.\overline{S^1_{high}})(S^2_{low}.\overline{S^2_{high}}).\overline{S_{littleveto}}.\overline{S_{inner\,halo}} \qquad (3.2)$$

The targets used were 0.25 g/cm^2 thick Au or S foils. As the flux of the beam was about $1.5 \cdot 10^6$ particles per spill, and the effective spill length is two seconds, the luminosity of the beam is $L = 6 \cdot 10^{26}$ cm^{-2}s^{-1}. The nuclear interaction cross-section for S + Au collisions is 3360 mb. Thus, an interaction rate of about 2000 reactions per second was measured during this experiment.

3.3 Zero-Degree Calorimeter

The Zero-Degree Calorimeter (ZDC) is designed to determine the energy loss of the incident beam particles by measuring the energy near a polar angle $\theta = 0°$. The ZDC has a sandwich-like structure of 60×60 cm^2 area uranium and scintillator plates. The calorimeter is located at 13.85 m from the target and has a length of 190 cm. The ZDC detects all particles coming from the target at very small angles, $\theta < 0.3° \cong \eta > 6$, where $\eta = -ln\tan(\theta/2)$ is the pseudo-rapidity. The detector consists of an electromagnetic part of 17 cm depth, equivalent to 20.5 radiation lengths (X_o), and a 172 cm long hadronic part, equivalent to 9.6 absorption lengths. Both the electromagnetic and hadronic energy can be measured using uranium and scintillator plates. The scintillator plates are read out via wavelength-shifter plates and light guides with 16 photomultipliers. The pulse height spectra of the ADC's were calibrated to the beam energy by adjusting the voltage of the 16 photomultiplier bases. They are summed and sent to a discriminator providing two logic signals, Z_{low} if a large amount of beam energy is missing, Z_{high} if the full beam energy is detected. The fast ZDC signal is combined with the Beam Counter, see section 3.2, and MIRAC, see section 3.4, to form the WA93 Trigger, see section 3.5.

3.4 MIRAC Calorimeter

The MId-RApidity Calorimeter (MIRAC) measures the transverse electromagnetic and hadronic energy in the kinematic region of mid-rapidity defined as half the beam rapidity. It is located at 11.25 m from the target and measures from $\eta = 6$ up to $\eta = 3$. It consists of four 1.32×1.20 m^2 blocks with a central hole of 10.5×10.5 cm^2. The electromagnetic part has a length of 5.6 radiation lengths or 0.6 hadron absorber lengths, made up by a stack of absorption and scintillator plates. Each block consists of 6×6 towers where each tower has an area of 20×20 cm^2. The towers are read out via wavelength shifting plates and light guides by photomultipliers. Using the calibration factor and position of a tower the transverse energy $E_T = E \sin\theta$ of the traversing particles can be measured for each event. The summation and angular weighting of the transverse energy is done for all measured particles in one event by hardware. The summed MIRAC transverse energy signal can be used for on-line trigger purposes. The energy resolution was $11\,\%/\sqrt{E(GeV)}$ for the electromagnetic part and $34\,\%/\sqrt{E(GeV)}$ for the hadronic part. The four inner towers, surrounding the beam pipe, were not used since frequently a signal above the highest energy threshold, most likely due to spectator particles from the beam, occurred. Three logic signals, M_{low}, M_{high}, and $M_{peripheral}$, are generated from the sum of the photomultiplier ADC signals. A signal M_{low} means very little energy measured in the MIRAC, M_{high} the opposite. The $M_{peripheral}$ was chosen to cover the intermediate region in transverse energy. The centrality of a collision is characterised by these three logical signals together with the ZDC, see section 3.3, and the beam counter, see section 3.2, and is expressed in the trigger signal, see section 3.5.

3.5 Trigger

The trigger signal characterizing the centrality of a collision is a combination of the logic signals from the beam counter, ZDC and MIRAC. The correlation between the measured ZDC and MIRAC energies is shown in figure 3.2. Measuring large transverse energy in the MIRAC and little forward energy in the ZDC corresponds to a central event. The necessity to study whether the reaction was central or peripheral arises from the fact that the quark-gluon plasma is expected to be observed most likely for central events. Here, large collision zones are created. The peripheral events correspond to well-known hadron-hadron collisions. The rate of events from the various trigger

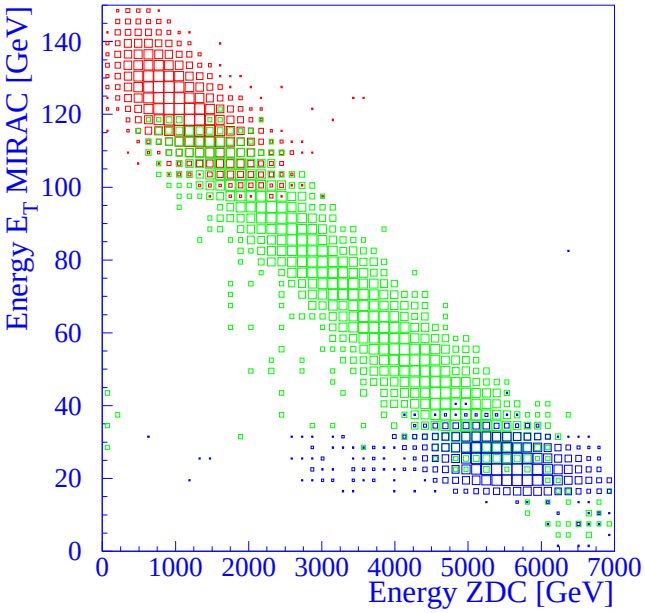

Figure 3.2: *Transverse energy measured in the MIRAC versus the forward energy in the ZDC for 200 GeV/nucleon S+Au reactions.*

Table 3.1: *Trigger definitions.*

Trigger Class	Trigger definition
E_THigh	$S_{validbeam} \cdot M_{high} \cdot M_{peripheral} \cdot M_{low}$
Minimum Bias	$S_{validbeam} \cdot M_{low}$
Semi Central	$S_{validbeam} \cdot \overline{M_{high}} \cdot M_{peripheral} \cdot M_{low}$
E_TPeripheral	$S_{validbeam} \cdot Z_{low} \cdot \overline{M_{peripheral}} \cdot M_{low}$
Beam	$S_{validbeam} \cdot Z_{high} \cdot \overline{M_{high}} \cdot \overline{M_{peripheral} M_{low}}$

classes E_THigh : E_TPeripheral : Semi Central : Beam = 1 : 1 : 3 : 2000 as determined from the composition of the least biased sample of reaction events (Minimum Bias). Using down-scaling factors for the various triggers the ratio of data taken for the respective triggers is 7 : 3 : 3 : 1. So roughly 50 % of the registered data are central events. The ZDC signal was removed in the on-line trigger analysis. Since the measured beam energy by the ZDC for the beam trigger started to degrade in the course of the experiment most

likely due to radiation damage of the ZDC. Further rejection criteria in the off-line analysis led to the following estimate of 1992 data, presented in table 3.2.

Table 3.2: *Number of events taken for the magnetic dipole field setting on or off.*

	S+Au Field On	S+Au Field Off	S+S Field On
E_TPeripheral	$1.0 \cdot 10^6$	$0.2 \cdot 10^6$	$56 \cdot 10^3$
Semi Central	$0.5 \cdot 10^6$	$83 \cdot 10^3$	$30 \cdot 10^3$
E_THigh	$1.2 \cdot 10^6$	$0.26 \cdot 10^6$	$70 \cdot 10^3$

3.6 Si-Drift Detector

In order to measure the charged-particle multiplicity and rapidity distributions a Si-Drift detector was implemented in the WA93 experiment. The pseudo-rapidity interval covered by this detector was that of the photon-multiplicity detector discussed in section 3.9. This coverage is required to obtain the N_γ/N_{ch} ratios, see section 2.4.

In the WA93 experiment a 320 μm thick circular detector with a 64 mm diameter, a central hole of 16 mm and 360 anode pads at the circumference was used. In Si-drift detectors [57, 58, 59] the negative electrical charge, caused by traversing ionizing particles, is transported over drift distances of several cm. An array of reverse biased p-strips on both sides of the high-resistivity n-type silicon fully depletes the bulk and maintains a gutter-like potential. The ionization-electrons created by charged particles are driven parallel to the surface towards the collecting anodes on the edge of the detector. Here, external amplifiers pickup the signal and transfer it to a gaussian shaper unit and flash ADC's for further processing. Since the drift velocity of the Si-wafer is known the position of the charged particles can be determined with a 20 μm resolution.

3.7 Streamer-Tube Detector

A large array of streamer tubes [57, 60] serves as a thin and efficient detector and provides a charged-particle veto signal for the lead-glass detector,

section 3.8, which measures photons.

The detector consists of two planes of streamer tubes STD_1 and STD_2 at a distance of 9.22 m and 9.38 m, respectively, from the target. A streamer-tube detector is made of arrays of PVC tubes with a square cross-section of 9×9 mm^2. In the center of the PVC tube a silver plated anode wire of 100 μm diameter is kept at a voltage of about 4750 volt. The tubes are flushed with a gas mixture of 30:70 % Argon-Isobutane at 1.2 bar.

In case a charged particle passes through a tube, electrons will be liberated and an avalanche will evolve close to the wire. The field will be distorted close to the wire and electrons can recombine under photon emission. Away from the wire this radiation will free electrons in the tube. The electrons will also take part in the avalanche in case they are close to the wire, otherwise recombinations take place. The extending ion cloud, called "streamer", may reach up to the cathode walls and is self-quenching due to the weaker field far from the wire. The walls of the tube are covered with a graphite layer in order to prevent electrons from being liberated from the walls that will cause multiple streamers. The streamer tubes are read out capacitively. The surface area of the streamer-tube planes is covered by 21 $\times$ 21 cm^2 sized printed circuit boards carrying 40 or 160 conducting pads facing the tubes. The 160-pad boards are used in the high multiplicity area, close to mid-rapidity, while the 40-pad boards are used in the outer regions of the STD planes. The two STD planes together contain about 40.000 pads.

3.8 Lead-Glass Spectrometer

One of the proposed interesting signals from the quark-gluon plasma is the observation of direct photons. In order to distinguish this signal from the enormous background coming from neutral meson decay (mostly π^0 and η) a high reconstruction efficiency is needed. This requires a photon detector with very good energy resolution and high granularity.

In WA93 three detectors with high position resolution were placed in a U shaped form. One was SAPHIR (Single-Arm Photon detector for Heavy-Ion Reactions) which had already been used in the WA80 experiment. It consists of 1278 $SF5$ lead-glass blocks of a length of 460 mm and an area of 35×35 mm^2 . The length is approximately equal to 18 electromagnetic radiation lengths and about 1 hadronic interaction length. Photomultipliers read out the modules at the back. The two other detectors TOWER1 and TOWER2 are positioned vertically on each side of SAPHIR. They cover $2.1 < \eta < 2.9$ in pseudo-rapidity at 10.06 m from the target. The towers

consist of 1260 modules of TF_1 lead glass each $4.0 \times 4.0 \times 40$ cm^3 in size. The length of 40 cm corresponds to 14.4 electromagnetic radiation lengths and about 1 hadronic absorption length ($\lambda_{SF5} = 46$ cm and $\lambda_{TF_1} = 38$ cm). Due to the limited absorption length $\approx 37\,\%$ hadrons cause a highly irregular shower, 63 % of the hadrons deposit energy according to a minimum-ionizing particle.

The energy resolutions of SAPHIR, TOWER1 and TOWER2 are similar and amount to $0.4\,\% + 6\,\%/\sqrt{E(GeV)}$.

The gain of the photomultipliers is monitored by a laser reference system. The laser itself is monitored using a reference photomultiplier calibrated by a ^{241}Am doped NaI crystal. The relative gain stability is better than 1 %.

3.9 Photon-Multiplicity Detector

The Photon-Multiplicity Detector (PMD) aims to select events with a high photon content. By a simultaneous measurement of the charged particle multiplicity, using the Si-drift detector, and of the photon multiplicity, the ratio of the number of photons over the number of charged particles can be studied, see section 2.4. An increased ratio might signal the formation of hot interacting hadronic matter or even the formation of the QGP.

The PMD, with a size of 200×160 cm^2 and located at 10.06 m from the target is a pre-shower device. Its angular coverage is $1^\circ < \theta < 6^\circ$. A conversion layer of 2 cm lead equivalent to 3.8 radiation lengths is used. This thickness has been chosen to optimize photon efficiency and minimize hadronic interactions.

The electrons are detected in the beginning of the shower by scintillating pads glued in closed-packet arrays on the converter sheet. For the inner area of 60×60 cm^2, with a central hole of 10×10 cm^2 to let the beam pass through, a pad size of 15×15 mm^2 is used, the remainder has 25×25 mm^2 pads. The signal of each pad is guided using a wavelength shifting fibre to a CCD (Charge Coupled Device) camera equipped with an image intensifier.

The 7600 pads are grouped in quadrants. A quadrant is read out by 1900 pads, yielding for each pad about 10-15 pixels at the CCD level. The CCD camera has a resolution of 145×218 pixels.

3.10 Charged-Particle Spectrometer

The charged-particle spectrometer was incorporated in the WA93 setup to study in detail through intensity interferometry the space-time evolution

of the hot hadronic system produced in the heavy-ion collision. Therefore the acceptance was chosen, together with that of the photon spectrometer, around mid-rapidity [61, 62, 63, 64].

The charged-particle spectrometer employs the large dipole magnet Goliath, with a 1.6 m pole gap and a 2 Tm bending power. The pole diameter is 2.2 m. The horizontally bent charged particle tracks are detected in four Multi-Step Avalanche Chambers (MSAC), each having a 1.2×1.6 m^2 sensitive area. The coordinate system for the WA93 experiment is defined as follows. The beam direction corresponds to the z-axis, the normal to the z-axis in horizontal direction corresponds to the x-axis and the vertical direction corresponds to the y-coordinate. The chambers are positioned, using the primary ionization gap as plane of reference and the z-coordinate, at z_1 = 425.6 cm, z_2 = 564.0 cm, z_3 = 689.4 cm and z_4 = 814.5 cm from the target. Each chamber covers $\pm$ 60 cm in the vertical and 160 cm in the horizontal direction. The sensitive areas of the four chambers closest to the beam line start at x_1 = 31.2 cm, x_2 = 40.5 cm, x_3 = 50.7 cm, and x_4 = 60.5 cm, respectively. The magnetic field strength was measured for a grid of spatial positions between and near the magnet poles. Further details are given in section 4.2.2. A measurement of the position of each track in the chambers and thus the direction of the tracks together with the knowledge of the magnetic field allows for the reconstruction of the momenta, see section 4.5, of negative charged particles.

The spectrometer has to fulfill several requirements. First of all it has to operate in a high-multiplicity environment, with 40 to 100 charged particles per m^2. A large acceptance of 1.5 units of rapidity around mid-rapidity was required. To be able to do intensity interferometry a high momentum resolution was needed. Furthermore, the system had to be of a light construction, in order not to disturb the photon measurements.

A magnetic spectrometer using MSAC chambers largely fulfills these demands. Particle identification, e.g. using a time-of-flight detector, was not implemented in the WA93 experiment. The upgrade WA98 has such a device. Therefore, the measurement of negatively charged particles was chosen in order to keep the amount of background tracks for the $\pi^-\pi^-$-correlations as low as possible. This is so because the yield of other negatively charged particles is small as compared with π^- whereas in case of positive charged particles there is a considerable admixture of protons to the yield of π^+. The MSAC chambers are gaseous ionization detectors [65, 66, 67]. In general, ionization detectors are based on the principle that incident radiation ionizes the compound which can be a gas, a fluid or a solid. The ionization is read out usually after amplification [68]. Gas-ionization detectors are widely

used in medicine, astrophysics and biology [69]. The MSAC chamber uses a gas-mixture of Neon and Tri-Ethyl-Amine (TEA), a photo-emissive gas, under atmospheric pressure [70, 71, 72, 73], allowing optical read out of this detector.

In the following subsections the design characteristics, the construction, section 3.10.1, and the optical read-out, section 3.10.2, will be discussed. Furthermore, the monitoring and operation, section 3.10.3, of these detectors will be outlined.

3.10.1 Construction and Principle of Operation

The Multi-Step Avalanche Chambers in the WA93 setup consisted of a sandwich of 18 1.2×1.6 m^2 frames. These detectors were developed by and built at the University of Geneva, Switzerland [61, 62, 63]. In fact a MSAC is a stack of three Parallel-Plate Avalanche Chambers (PPAC). One MSAC has twelve electrodes which are called meshes, as schematically shown in figure 3.3. A mesh consists of crossed stainless steel wires, equally spaced at a distance of 500 μm and each having a 50 μm diameter. The frames are made of a very light composite of vetronite, honeycomb and foam. Using this composite, the frames have a total thickness corresponding to only 10 % of a radiation length and the meshes have in total 0.7 % radiation length.

The frames span the meshes with a tension of 15-50 kg/m. Such a tension is needed because the parallelism of the electrodes is a critical factor for the operation of the PPAC. It should be better than 20 μm for the 4 mm amplification gaps. Special care is taken to prevent sparking at the edges of the chambers where the electromagnetic field is not homogeneous. A 0.5 mm thin vetronite strip protruding 5 mm inside the chamber volume is used. To secure the wanted parallelism ceramic spacers with the same geometry have been used.

When a charged particle passes through the first gap of the MSAC mesh 1 and 2, primary ionization is produced, see figure 3.3.

The Coulomb interaction between the electromagnetic field of the particle and the gas atoms is the dominant process for the ionization. The average energy loss of a charged particle crossing a thin medium is described by the Bethe-Bloch formula [68]. The particles crossing the MSAC chambers are mostly minimum-ionizing-particles (MIP). The energy loss in Neon gas would be 2.71 keV cm^{-1}. The thickness of the first ionization gap is 11 mm, leading to an average energy loss of the MIPs is 3.0 keV. In a thin layer of material, like the Neon gas in the first ionization gap, the total energy-loss distribution of a traversing charged particle is determined by a small amount

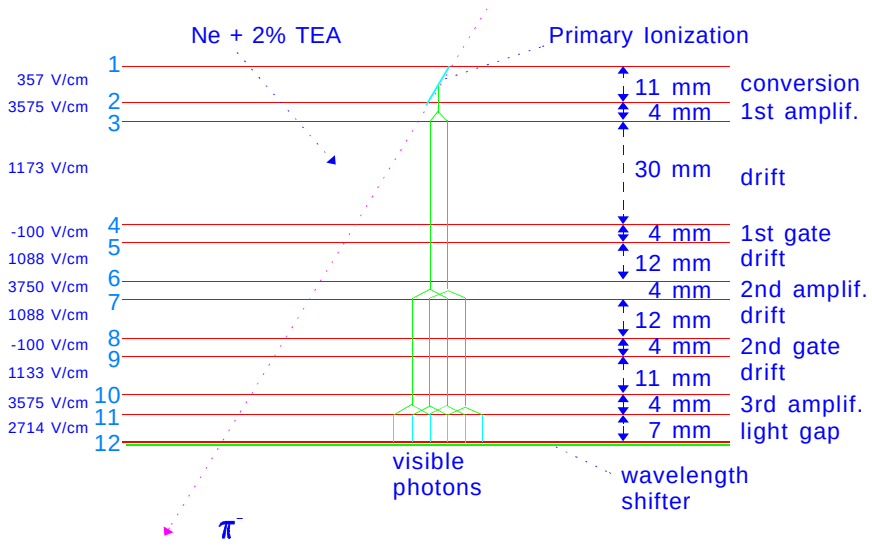

Figure 3.3: *Side view of the meshes in a MSAC chamber.*

of interactions. The interaction of the charged particles is characterized by large fluctuations in a wide range of energy transfer. The energy loss distribution of the hits in the gap can theoretically be described by a Landau distribution [68]. The Landau distribution is asymmetric and has a high energy tail, caused by close collisions between the crossing charged particles and the gas electrons. The amount of primary ionization can largely fluctuate due to this distribution. The average amount of energy lost for 1 ion-electron pair is 36 eV for Ne. Therefore, about $3000/36 = 80$ ion-electron pairs will be created on average.

The small electron cloud drifts under the influence of the applied E-field into the amplification gap of 4 mm. In this first-stage amplification the number of electrons is increased by a factor of $10^4 - 10^5$. This multiplication in gas detectors occurs, when the primary ionization electrons gain sufficient energy from the accelerating field to further ionize the gas atoms and is described by

$$M = \frac{e^{\alpha \cdot d}}{1 - \gamma \cdot (e^{\alpha \cdot d} - 1)} \tag{3.3}$$

where $\alpha(p, T, E)$ is the Townsend coefficient which depends on the pressure p, the temperature T, and the average ionization energy E of the gas. The factor γ takes into account the effect of positive ions hitting the cathode wire and creating electrons due to the photoelectric effect, and is usually small. Although the multiplication, as described by the above formula, seems to rise without limit, in reality at multiplications of 10^8 breakdowns due to the creation of a plasma column occur.

The electron cloud passes into a drift gap. Diffusion of the electrons in this gap, reducing the charge density, prevents breakdown in further stages. Furthermore, the image is stored, using the typical electron drift time of about 1 μs, allowing the trigger logic to decide, whether or not to open the 4 mm gate gap. Normally the gate gap is biased by a reverse voltage of 50 V. The trigger generates with a delay of 0.7 μs and gate width of 800 ns a 300 V opening pulse for the gate gap (the drift speed of electrons is 3.2 $cm/\mu s$ in saturation).

The operation of the MSAC in trigger mode has the advantage that unnecessary discharges, e.g. due to cosmic radiation, do not occur. This prevents positive-charge buildup and, with respect to the mentioned subject of sparking, improves the performance. After the first gate the electrons enter a 12 mm drift gap with drift time $\approx 0.5 - 1.0\ \mu s$. The transfer into these weaker fields leads to an electron loss by a factor $E_{ampl}/E_{drift} \approx 5$. Another 4 mm amplification gap, a 12 mm drift gap and a 4 mm gate gap follow. This second gate is triggered 1.6 μs after the event and has a gate width of 800 ns. Another 11 mm drift gap and 4 mm amplification gap follow. Directly after this amplification gap the 7 mm light gap has been placed to maximize the number of emitted photons by excited TEA molecules [70, 71, 72, 73]. TEA is a very good quencher due to 2 electrons which are easily excited and de-excite by emitting UV light. Both excitation and recombination and thus light emission do not occur in intense electric fields. The main four orders of magnitude of the light intensity originate from the light gap where the electric field is lower. Here, the mechanism of excitation of TEA gas molecules prevails over ionization of the Ne gas atoms. To adapt the emitted light spectrum, peaked at 280 nm, to the sensitivity peaked at 400 nm of the CCD-camera a 1 mm thick wavelength shifter absorbs the UV light and re-emits it in the blue range of the spectrum. The number of isotropically emitted photons is about 10^6. The photons are reflected, via aluminized mylar foil mirrors, positioned at 45° with respect to the chamber surface, into the solid angle of the CCD cameras.

The MSAC chambers are constantly flushed with a mixture of Neon and TEA. TEA is a poisonous gas and highly inflammable. It is kept liquid at 0°

C. The refilling of TEA takes place under strong security precautions. Both rubber gloves and gas masks have to be worn. By bubbling Neon through the TEA liquid a mixture of Neon and 2% TEA is fed into the chambers.

Each chamber has an entrance and an exit window consisting of two 50 μm thick mylar foils 10 mm apart with a constant Ar gas flow in between. This shielding prevents air from entering the chamber, which would disable proper operation.

3.10.2 Optical Readout

Signals from each chamber are optically read out by two image intensified CCD cameras. In front of the CCD chip of 288×385 pixels, each having 6 intensity-bits, two image intensifiers amplify the light signal. The first image intensifier is a micro-channel plate, where light falling on a S25 photocathode is converted into electrons. Each 18 mm long micro-channel is a metal coated glass channel placed under an angle with respect to the applied $E-$field of 9 kV. The electrons will, by bouncing through a channel, multiply by liberating electrons from the metal coating. The electrons are directed to a fast phosphor screen. The emitted photons enter a de-magnifying electrostatic image intensifier used as an active taper, to reduce the image by a factor 1.7. The emitted light shines on the CCD Image Sensor. This analog circuit converts the optical image into electronic output. Each element (pixel) consists of a voltage gated np-junction (Photo MOS/ Photo Diode). The light will create electron-hole pairs in the p-type material. The electrons travel to the n-type material under the applied gate-voltage. Here, the accumulated photo-charges are stored after which these charges are read out as a voltage signal which is amplified and finally digitized. The CCD data, containing 18 bit position and 6-bit ADC value information, are stored using 24-bit words into Memory-CCD processors. Each MCCD processor has 2 memories, A and B, each of 1 Mb size. Certain thresholds (pedestal values) for the pictures are set (ADC level, maximum number of pixels) to reduce the final data rate. The filtered information is stored through a VSB bus into FIC 8230 processors (operating under OS9); see section 3.11 and figure 3.4. Between the effective spills the data are accessed via VME by the main acquisition system. The allowed event rate is 50 Hz.

3.10.3 The Light Monitoring System

Like all detectors the MSAC chambers have operation limitations. First of all, they are influenced by weather conditions. The atmospheric pressure

and temperature have an effect on the electron multiplication. Moisture in the air causes gas ionization on the edges of the chambers. A third tendency of the chambers is to have complete breakdown, i.e. sparking.

The light output of the chambers is automatically controlled by the following monitoring system. A ^{90}Sr (Strontium) β^- source (0.5 MeV and 2.1 MeV) is placed on one side of the chamber. Each time that a scintillator equipped with a trigger photomultiplier on the other side of the chamber measures an electron, another photomultiplier measures the light output of the chamber. If the light output changes with respect to the reference gain, the voltage across the three amplification gaps, which is typically about 1420 V, is automatically adjusted. The gas breakdown, called corona, due to moisture causes currents to be drawn from the high voltage (HV) supply. This degrades the performance of the chambers and might ruin the chambers, due to fire hazard. This effect disappears by lowering the HV or shutting down the chamber. Giving the chamber an extra layer of insulating paint does only solve the problem temporarily. In the follow-up experiment WA98 the coronas have not been observed.

Sparking of MSAC chambers is an effect which has been known for a number of years. It degrades their performance enormously, because after each breakdown the HV has to run up to its previous value. The dead-time due to this effect was about 500 ms. By the application of zener-diodes the dead-time could be reduced to about 200 – 250 ms. The zener-diodes drain the excessive charge each time there is a spark, thus facilitating the recovery of the HV-level. Sparking for MSAC's is related to the very high electron density in an avalanche. The multiplication is of the order 10^8. This is the region where breakdown is known to occur. Most likely highly ionizing particles or fluctuations of the primary ionization, due to the Landau distribution, cause the electron densities to exceed the breakdown limit. The high electron density causes a plasma column that locally increases the field. Breakdown due to VUV emission, related to recombination of fragmented hydrocarbons, does not seem to be important for PPAC chambers. The VUV light is known to ionize the gas locally. This kind of ionization is also a function of the electric field, as has been observed for multi-wire and proportional chambers [72, 74].

In the MSAC monitoring system a "spark photomultiplier" measuring the light flash warns the operator to adjust the voltage in case of excessive sparking. The maximum tolerable amount of sparking in the WA93 experiment, for a particle flux of about 40 particles per chamber, was set to about 10 % sparking probability per chamber per burst of about 100 events.

3.11 Data-Acquisition System

The signals from the detectors are digitized in the experiment for each event in modules residing in CAMAC, Fastbus and VME. The modules are communicating in a VME multiprocessing system running the OS9 operating system. One CPU, an ELTEC E6, acts as the main event builder and synchronizes the readout of the others. In case of a period of no effective spill or a full memory module, the data from the 10 E6 and 3 CES FIC8232 are fetched by the event builder and written to video 8 mm tapes, with a capacity of 2 Gb using Exabyte 8500 tape drives. The respective CPU's perform pedestal subtraction and zero suppression in order to reduce the data stream. A schematic drawing of the MSAC data-acquisition system is shown in figure 3.4. The whole process is monitored by the online program

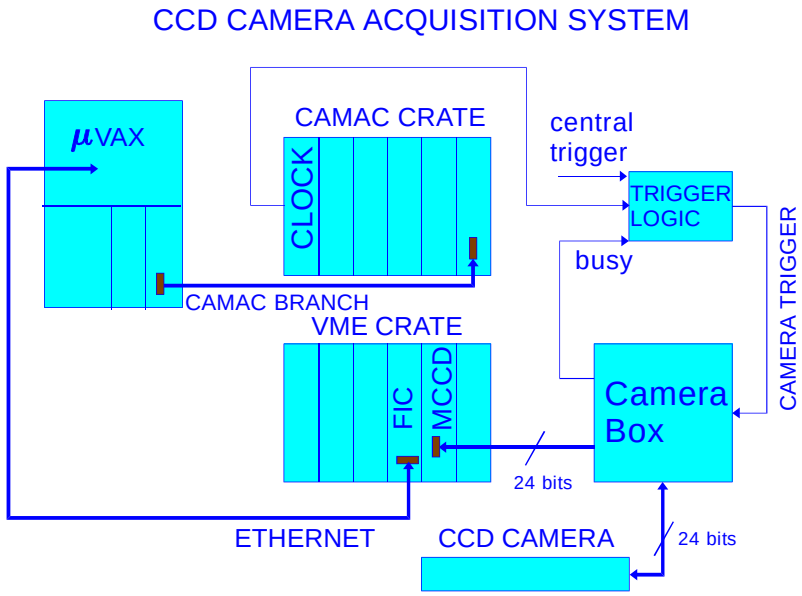

Figure 3.4: *Data-acquisition system for the MSAC chambers. From the FIC the data is transported to the event builder in the main data-acquisition system.*

MONA running on a VAX host computer. From here the process of data

taking can be altered, stopped and started. Warnings from the respective modules are displayed in case user intervention is needed. Using an Ethernet connection to the main event builder, the data stored in a ring buffer can be partially retrieved to workstations. Spectra are studied here to insure that the detectors are functioning properly.

3.12 PAD Chamber

The CCD camera readout system was found to have several severe limitations:

- The MSAC chambers have to yield about 10^7 electrons in order to achieve a large enough light output of 10^7 photons detectable by the CCD cameras. Breakdown due to the Landau tail of the distribution for the electron yield is likely to occur.
- Sparking yields a dead time of the high voltage system of about 250 ms, thus reducing the efficiency of the tracking system.
- The CCD cameras operate at the limit of their sensitivity. There are indications that on the outer parts of the chambers the cameras are less efficient.
- The CCD cameras are limited in their readout speed to 50 Hz and can not keep up with the 1000 Hz data taking rate of the other detectors in the experiment.
- There are indications that satellite hits, see section 4.3, can be related to either the behaviour of the CCD chip or multiple avalanches in the MSAC chamber.

An improved readout method was developed for the WA98 setup. The method consists of directly measuring the charge resulting from the avalanche multiplication. Copper elements, pads of 1×16 mm^2, are used to cover the back plane of the MSAC with 1.2×0.8 m^2 surface. The resulting amount of 57360 pads are read out at high speed allowing the data to be present in VME after 1 ms.

A special chip with 16 pad inputs was designed; see figure 3.5. The chip contains 16 charge-integrating amplifiers (0.5 V/pC). The amplifiers are gated by a 100 ns trigger and feed their output to both an analog 16 fold multiplexer and a summed trigger. A non-linear amplifier, gain = 6, feeds the outputs to a flash ADC. The converted signals are stored into

7-bits wide and 16 words deep FIFO buffer (6-bits data + 1 parity bit). The total time to convert all 16 channels is designed to be 16 times 2 μs. Subsequently the digitized signal data will be shifted via a bus line between the connected FIFO's into the memory of a Digital Signal Processor (DSP 2101) at the clock speed of 12.5 MHz. In the chip design the digitized part

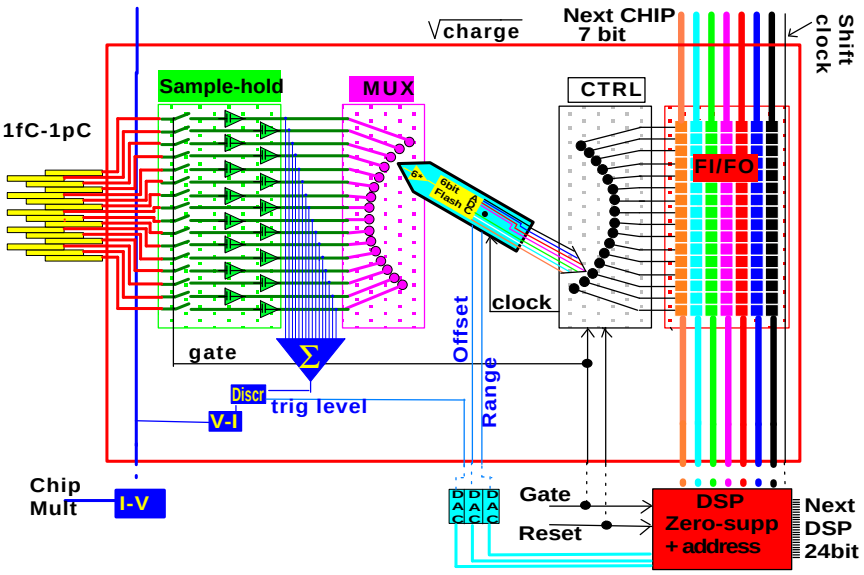

Figure 3.5: *Layout of charge-sensitive chip, with the analog part at the left and the digital part at the right. The analog signal is converted by a 6-bits flash ADC in the middle.*

has been separated from the analog part. The chip surface area is $\approx$ 14 mm^2 which is $\approx$ 6% of the total PAD area. The dissipation will be 25 mW of which the analog part contributes 20 mW and the digital part 5 mW. The maximum temperature under which the chip can operate is 80 °C. An estimate of the temperature, using Stefan-Boltzmann black-body radiation temperature, assuming the heat, dissipated by the chips to be uniformly spread over the PAD plane, yields 36.2 °C. This temperature rise has been experimentally verified.

The construction of the PAD chamber consists of two stages of amplification, having a similar design as the MSAC chamber, with the addition of a special drift gap and Faraday cage for the PAD plane. The PAD chamber,

see figure 3.6, has a size of 1200 mm by 800 mm (inner dimensions). The PAD plane is covered by 25 boards, 48 mm wide and 800 mm long. Each board has 3 chains of 48 chips each reading 16 horizontally staggered pads. Each chain of 768 pads is read out by 1 DSP (total number of DSP's 75). The vertical bus contains 7 data bits, reset and clock signals, analog ADC levels and the gate signal. The DSP will perform zero suppression. It is

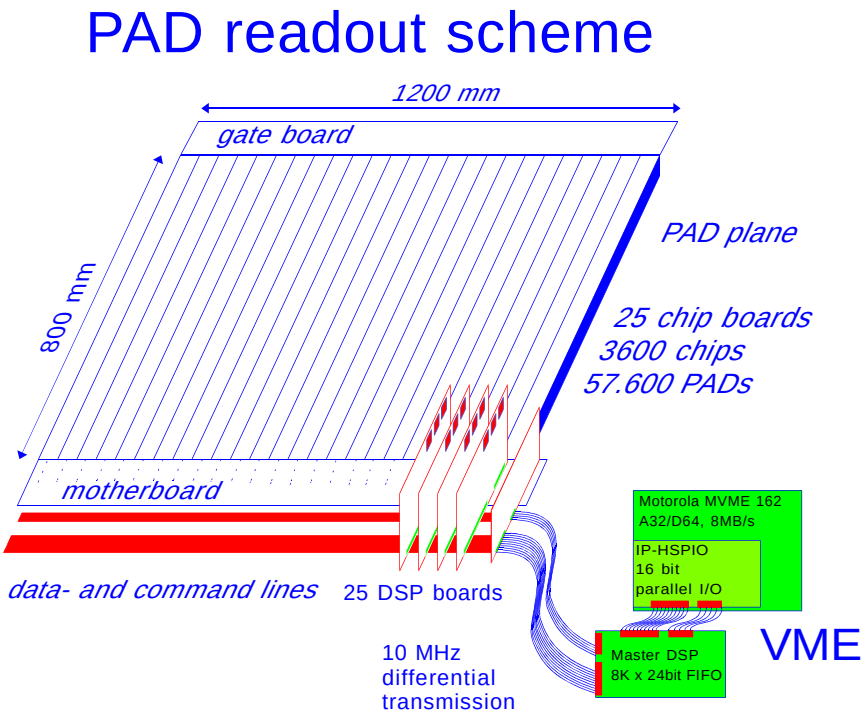

Figure 3.6: *Layout of the pad chamber. The twenty-five chip boards are read by twenty-five DSP boards mounted on the mother board.*

expected that at most an occupancy of 4 % of the total amount of pads will be measured. This data is shifted to a FIFO buffer on the DSP board and in case all data have been processed the DSP signals that it is ready. If all the DSP's have signaled to be ready the transceiver card on the mother board, containing all the DSP's board, shifts the data from the 75 DSP's to the VME board containing an 8 Kb (24 bit) FIFO buffer, a master DSP and a VME processor. As long as the FIFO on VME has enough memory space

the transceiver keeps sending the data. When all the data have been read-out the VME processor starts a DMA transfer to a VME memory module containing a Motorola processor. The main event builder running on an E7 processor can fetch them whenever this memory module is running out of space. The performance of a test PAD readout system has been measured [75] yielding a lower limit of 94 % efficiency of the chamber.

3.13 Summary

In the previous sections the WA93 setup has been described. The basic aim of the WA93 experiment is the measurement of the direct photons together with knowledge of the space-time evolution from the measurement of negatively charged particles. The experiment was developed and performed by an international collaboration of institutes. Each institute was involved with one or several of the detectors. The author was, as a member of the KVI Groningen team together with the teams from the University of Lund and the University of Geneva, particularly involved with the charged-particle spectrometer. The MSAC chambers were developed and built by the University of Geneva. Participation in the construction, testing and operation of these chambers gave particular insight into the performance characteristics of these sensitive devices. The sparking problem for the WA93 experiment could partly be solved by the implementation of zener diodes.

The development and testing of the prototype PAD chamber for the WA98 experiment was done together with the University of Lund and involving the companies CTI Groningen for the development of the DSP readout and Sicon Linköping for the design of the VLSI chip. The DSP readout was extensively tested at the KVI. Especially initial malfunctioning problems of the VLSI chip were investigated at the KVI and solved.